ACS APPLIED MATERIALS & INTERFACES

Research Article

www.acsami.org

Structural, Optical, and Dielectric Properties of $Bi_{1.5-x}Zn_{0.92-y}Nb_{1.5}O_{6.92-\delta}$ Thin Films Grown by PLD on R-plane Sapphire and $LaAlO_3$ Substrates

A. Le Febvrier,[†] A. C. Galca,*[,‡] Y. Corredores,[§] S. Députier,*[,†] V. Bouquet,[†] V. Demange,[†] X. Castel,[§] R. Sauleau,[§] R. Lefort,[∇] L.Y. Zhang,[#] G. Tanné,[#] L. Pintilie,[‡] and M. Guilloux-Viry[†]

[†]Institut des Sciences Chimiques de Rennes, UMR-CNRS 6226, Université de Rennes 1, 263 av. Gal Leclerc, 35042 Rennes, France

[‡]National Institute of Materials Physics, Atomistilor 105 bis, 077125 Magurele, Ilfov, Bucharest, Romania

[§]Institut d'Electronique et de Télécommunications de Rennes, UMR-CNRS 6164, Université de Rennes 1, IUT de Saint-Brieuc, 18 rue H. Wallon, 22004 Saint-Brieuc, et 263 av. Gal Leclerc, 35042 Rennes, France

[∇]Institut de Physique de Rennes, UMR-CNRS 6251, Université de Rennes 1, 263 av. Gal Leclerc, 35042 Rennes, France

[#]Laboratoire en Sciences et Techniques de l'Information, de la Communication et de la Connaissance, ISSTB, UMR-CNRS 6285, Université de Bretagne Occidentale, 6 av. V. Le Gorgeu, 29238 Brest, France

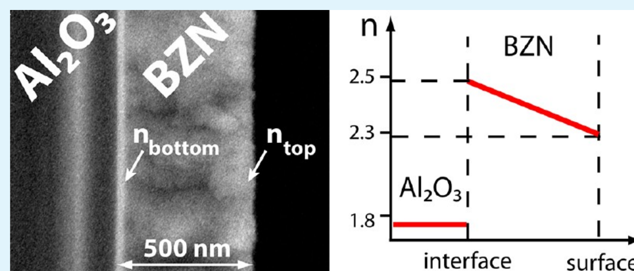

ABSTRACT: $Bi_{1.5-x}Zn_{0.92-y}Nb_{1.5}O_{6.92-\delta}$ thin films have the potential to be implemented in microwave devices. This work aims to establish the effect of the substrate and of the grain size on the optical and dielectric properties. $Bi_{1.5-x}Zn_{0.92-y}Nb_{1.5}O_{6.92-\delta}$ thin films were grown at 700 °C via pulsed-laser deposition on R-plane sapphire and $(100)_{pc}$ $LaAlO_3$ substrates at various oxygen pressures (30, 50, and 70 Pa). The structure, morphology, dielectric and optical properties were investigated. Despite bismuth and zinc deficiencies, with respect to the $Bi_{1.5}Zn_{0.92}Nb_{1.5}O_{6.92}$ stoichiometry, the films show the expected cubic pyrochlore structure with a (100) epitaxial-like growth. Different morphologies and related optical and dielectric properties were achieved, depending on the substrate and the oxygen pressure. In contrast to thin films grown on $(100)_{pc}$ $LaAlO_3$, the films deposited on R-plane sapphire are characterized by a graded refractive index along the layer thickness. The refractive index (n) at 630 nm and the relative permittivity (ε_r) measured at 10 GHz increase with the grain size: on sapphire, n varies from 2.29 to 2.39 and ε_r varies from 85 to 135, when the grain size increases from 37 nm to 77 nm. On the basis of this trend, visible ellipsometry can be used to probe the characteristics in the microwave range quickly, nondestructively, and at a low cost.

KEYWORDS: *BZN, defect pyrochlore, thin film, PLD, spectroscopic ellipsometry, optical properties, dielectric properties, graded layer*

INTRODUCTION

Microwave devices based on dielectric thin films have been implemented for several years for various applications for the purpose of facilitating tunability, such as planar capacitors, phase shifters, tunable filters, or coplanar waveguides.[1] Such applications require materials with a high permittivity, a low dielectric loss, a low leakage current, and a high tunability. Among dielectric materials, the ferroelectric family has been studied[2,3] extensively, compared with other dielectrics, such as compounds with a pyrochlore structure, which show potentiality for their integration into microwave devices. Recent works have demonstrated that the bismuth zinc niobate cubic pyrochlore is an attractive candidate for microwave applications.[4−6] This compound belongs to the relaxor family, i.e., its dielectric properties depend on both temperature and frequency.[7] $Bi_{1.5-x}Zn_{0.92-y}Nb_{1.5}O_{6.92-\delta}$ thin films deposited by various processes, such as the metallorganic decomposition method,[8] the magnetron sputtering technique,[5,9,10] or pulsed-laser deposition (PLD),[11,12] show a moderate permittivity (typically 150−200), a very low dielectric loss, and a high tunability up to 55% (under a high electric field of 2.4 MV/cm).[5] In the case of the PLD process, several studies have shown that the structure and microstructure depend on the deposition parameters, which involve a strong modification of their dielectric properties.[12−15] In the literature, bismuth zinc niobate stoichiometric targets were used but only few analyses that are related to the composition of the thin films have been reported.[12,16] Bismuth and zinc deficiencies cannot be ruled out. Therefore, we have chosen to name the cubic pyrochlore with the "$Bi_{1.5-x}Zn_{0.92-y}Nb_{1.5}O_{6.92-\delta}$" general formula (BZN). Zhang et al.[12] have described the influence of the deposition temperature on the morphology and composition of the films,

Received: June 25, 2012
Accepted: September 20, 2012
Published: September 20, 2012

© 2012 American Chemical Society

and the consecutive variations of their dielectric characteristics. Sundheendran et al.[14] have studied the effect of post-deposition annealing on the morphology and dielectric properties of thin films deposited by PLD at room temperature under various oxygen pressures. However, only a few papers have reported the influence of the oxygen deposition pressure on the film characteristics, and especially its impact on their dielectric and optical properties. For example, the influence of oxygen pressure, ranging from 5 Pa to 50 Pa, on the dielectric characteristics (1 kHz−1 GHz band) has been investigated for $Bi_{1.5}Zn_1Nb_{1.5}O_7$ thin films grown by PLD on Pt(111)/TiO_2/SiO_2/Si(100) substrates.[15] It has been demonstrated that the deposition pressure governs together the crystallization, the preferential orientation, and the microstructure (shape of grains, grain size, and growth rate) of the thin films, and consequently, the dielectric properties.

In the present work, $Bi_{1.5-x}Zn_{0.92-y}Nb_{1.5}O_{6.92-\delta}$ (BZN) thin films were grown by PLD on R-plane sapphire and $(100)_{pc}$ $LaAlO_3$ (LAO) substrates. These substrates have been selected because of their low relative permittivity ($\varepsilon_r \approx 10$ and 24, for sapphire and LAO, respectively) and low dielectric loss ($\tan \delta \approx 10^{-4}$), which may be suitable for microwave devices. Their structural characteristics are expected to promote the epitaxial-like growth of the BZN pyrochlore films. The effect of the oxygen deposition pressure on the structural quality (in particular, orientation), the microstructure (focused on grain size, growth rate and density), and the dielectric and optical properties of the thin films were investigated. The relationship between the dielectric properties in the gigahertz range and optical properties versus grain size were discussed more specifically.

■ EXPERIMENTAL SECTION

Material. BZN thin films were deposited by pulsed-laser deposition (PLD), using a KrF excimer laser (λ = 248 nm). A stoichiometric target of the cubic $Bi_{1.5}Zn_{0.92}Nb_{1.5}O_{6.92-\delta}$ phase ($x = y = 0$) was first synthesized and sintered via a conventional ceramic route using Bi_2O_3, Nb_2O_5, and ZnO precursor oxides. Similar to the process described by Valant et al.,[17] the mixture was homogenized, pressed uniaxially into pellets and prereacted at 650 °C for 4 h. During this first step, Bi_2O_3 reacted with Nb_2O_5 and ZnO to form intermediate compounds, which prevent bismuth volatility in view of the higher treatment temperatures. In a second step, the powder was calcinated four times at 950 °C for 4 h, with intermediate grinding. Finally, the calcinated material was pressed uniaxially at 180 MPa into pellets and sintered at 1050 °C for 2 h. X-ray diffraction (XRD) confirmed the presence of the single-phase pyrochlore, referring to ICDD Powder Diffraction File (PDF) Card No. 052-1770. The deposition parameters were as follows: fluence, 2 J/cm^2; frequency, 2 Hz; temperature, 700 °C; target−substrate distance, 55 mm; and deposition time, 20 min. The deposition temperature was controlled during the thin film growth by a thermocouple placed on the substrate holder. Oxygen was introduced inside the deposition chamber under various pressures: 30, 50, and 70 Pa. The thin films were grown on R-plane sapphire and $(100)_{pc}$ $LaAlO_3$ (LAO). Note that this last orientation refers to the commonly used pseudo-cubic subcell, whereas LAO is actually rhombohedral. The deposition temperature was chosen to obtain 100 high-oriented thin films on both substrates.

Material Characterizations. For XRD analysis, two diffractometers were used: a D8 Advanced Brüker AXS ($\theta-2\theta$ configuration) equipped with a monochromatized Cu Kα_1 radiation source and a four-circle texture instrument (D8 Discover Brüker AXS) equipped with a parallel beam Cu Kα_1 radiation in $\theta-2\theta$, ω, and φ scan modes. Surface morphology and thickness were determined via field-emission scanning electron microscopy (FE-SEM), using a JEOL JSM 6310F system working at a low accelerating voltage (7 kV). The composition of the films was analyzed by energy-dispersive X-ray spectroscopy (EDS), using a JEOL JSM 6400 scanning electron microscope equipped with an ISIS Oxford analyzer (10 kV was used as an accelerating voltage and 10 nA as a beam current). A Horiba Jobin−Yvon UVISEL spectroscopic ellipsometer was employed to investigate the optical properties between 300 nm and 1200 nm. The measurements were performed at an incident angle of 65°. The optical model used to fit the experimental data was a three-layer model corresponding to the substrate, the thin film, and a rough top layer. A Cauchy dispersion[18] ($n = A + (B/\lambda^2)$) with or without a linear evolution (graded layer) of the refractive index was used to define the optical properties of the thin films. The fitting routine was performed in the spectral range where the film is transparent (the extinction coefficient k is zero, i.e., in the 500−1100 nm range). Measurements at microwave frequency were performed using three 50-Ω coplanar waveguide (CPW) transmission lines of various lengths (3, 5, and 8 mm), which were designed by using the electromagnetic Ansoft HFSS software, and manufactured using a standard photolithographic process. First, an ultrathin titanium film (5-nm-thick) and a 2-μm-thick silver overlayer were deposited on the BZN films by RF sputtering at room temperature. The titanium film ensured a strong adhesion of the silver layer. Then, a photolithographic technique and a wet etching operation were used to pattern the lines. The widths of the gap and central conductor of the CPW lines were equal to 40 and 60 μm on BZN/R-plane sapphire, and to 55 and 30 μm on BZN/$(100)_{pc}$ LAO, respectively. These dimensions were defined for matching the line impedance to 50 Ω, according to the substrate dielectric permittivity. Note that the metal deposition and photolithographic process, which are both carried out at room temperature, prevent interdiffusion and/or desorption problem(s) of the samples. The microwave measurements were performed at room temperature in X-band (~10 GHz) using a vector network analyzer (VNA 37369A Wiltron) and a probe station (Karl süss) with a tip spacing of 200 μm. The line-reflect-match calibration was carried out with a standard coaxial kit. The complex propagation constant γ^* (and, thus, the complex effective permittivity $\varepsilon^*_{eff} = \varepsilon'_{eff} + i\varepsilon''_{eff}$) of the transmission lines was calculated from the measured scattering parameters S_{11} and S_{21}. This enabled one to compute the dielectric permittivity ε_r of the BZN film using an analytical model based on the conformal mapping method for ferroelectric/dielectric heterostructures.[19] This model takes into account the transmission line dimensions, as well as the thicknesses of the BZN film and of the substrate. Further details are given in refs 19 and 20.

■ RESULTS AND DISCUSSION

Structure and Microstructure. The composition of the thin films, deposited on both substrates from a stoichiometric target, was $Bi_{1.3}Zn_{0.5}Nb_{1.5}O_{6.92-\delta}$ ($x = 0.2$; $y = 0.42$), and no significant difference regarding the cation composition was observed between the samples, regardless of the oxygen deposition pressure (30, 50, or 70 Pa). The difference in composition between target and thin films has already been noticed.[16] It is due to the volatility of bismuth and zinc at a high temperature and low pressure. The XRD patterns of the BZN films, deposited on both substrates at the mentioned oxygen pressures, are represented in Figure 1. Despite the Bi and Zn deficiencies, $\theta-2\theta$ patterns evidenced the possibility to achieve single-phase BZN thin films. The diffraction peaks were indexed in the cubic pyrochlore structure with a cell parameter equal to 10.558 Å ± 0.004 Å, which is close to the value of the bulk material[21] (ICDD PDF Card No. 052-1770). The XRD patterns show that the films were mostly oriented in the (100) direction with some (111) and (110) oriented crystallites. On both substrates, the increase in oxygen pressure led to a decrease of the intensities of the peaks related to the secondary orientations. The ratio of (hkl)-oriented grains of BZN (X_{hkl}) was estimated by the following formula (eq 1):

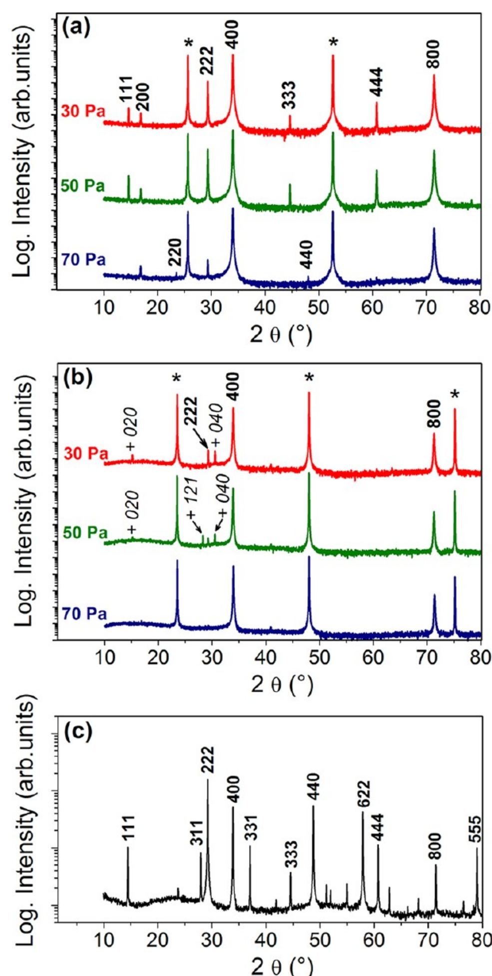

Figure 1. $\theta-2\theta$ XRD patterns of the BZN thin films grown on (a) an R-plane sapphire substrate; (b) a $(100)_{pc}$ $LaAlO_3$ substrate; and deposited under oxygen pressures of 30, 50, and 70 Pa. Peaks marked with a cross (+) and an asterisk (*) are related to $BiNbO_4$ (ICDD PDF Card No. 16-0295) and to the substrates, respectively. For comparison, the XRD pattern of the used target is given in diagram (c).

$$\frac{X_{hkl}}{X_{222}} = \frac{(I_{hkl})_{\text{film}}/(I_{hkl})_{\text{bulk}}}{(I_{222})_{\text{film}}/(I_{222})_{\text{bulk}}} \quad \text{and} \quad \sum X_{hkl} = 1 \tag{1}$$

where $(I_{hkl})_{\text{film}}$ is the normalized integral intensity of the (hkl) diffraction peak, which is equal to the integral intensity of the ω-scan peak multiplied by the full width at half maximum (FWHM) of the (hkl) peak on the $\theta-2\theta$ pattern; $(I_{hkl})_{\text{bulk}}$ is the integral intensity of the bulk material peak after correction, according to the multiplicity of 1, corresponding to oriented film or single-crystal reflections.

The proportions of each orientation are listed in Table 1. On both substrates, thin films were mainly composed of a high fraction (85%−100%) of (100) orientation. The in-plane ordering of the (100) oriented BZN films was also probed by φ-scans (see Figure 2). An epitaxial-like growth of BZN was evidenced with the four peaks separated by 90°. The FWHM of the φ-scan reflection peaks ($\Delta\varphi$) of the BZN films grown on sapphire ranged from 1.8° (70 Pa) to 3.1° (30 Pa). Thin films on LAO showed a better in-plane ordering quality, with $\Delta\varphi$ ranging between 0.4° (30 Pa) and 0.5° (70 Pa). This improvement of the structural quality shown by the φ-scans

Table 1. Relative Ratios of (hkl)-Oriented Crystallites and (100) Out-of-Plane Ordering Quality ($\Delta\omega$) for Thin Films Grown on R-Plane Sapphire and on $(100)_{pc}$ $LaAlO_3$ Substrates under Various Oxygen Deposition Pressures (30, 50, and 70 Pa)

substrate	oxygen pressure (Pa)	ratio of (hkl) orientation: (100)	(111)	(110)	out-of-plane ordering: $\Delta\omega$ of the 400 reflection
R-plane sapphire	30	85%	15%		1.4°
	50	95%	5%		0.3°
	70	∼100%	<1%	<1%	0.3°
$(100)_{pc}$ $LaAlO_3$	30	98%	2%		0.4°
	50	∼100%	<1%		0.3°
	70	100%			0.3°

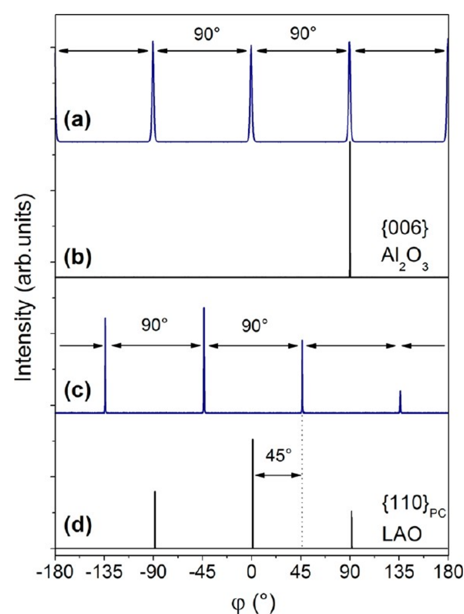

Figure 2. φ-scan XRD patterns performed on the {440} reflections of (100) oriented BZN thin films grown on (a) an R-plane sapphire substrate; (c) a $(100)_{pc}$ $LaAlO_3$ substrate; and deposited under an oxygen pressure of 70 Pa. φ-scan XRD patterns of the substrates performed on (b) the {006} reflections of Al_2O_3 and (d) the $\{110\}_{pc}$ of LAO.

is consistent with the ω-scan measurements (see Table 1). The high quality of the epitaxial-like growth could be explained by the calculated in-plane lattice mismatch, which was close to −1.5% between the BZN cubic pyrochlore and the LAO substrate and is defined by:

$$\frac{a_{(\text{BZN})} - 2 \times a'_{pc(\text{LAO})}}{2 \times a'_{pc(\text{LAO})}} \quad \text{with}$$

$$a'_{pc(\text{LAO})} = a_{pc(\text{LAO})} \times \sqrt{2} = 5.359\ \text{Å} \tag{2}$$

Considering a rectangular lattice for the R-plane sapphire, with $a'_{Al_2O_3} = 5.12$ Å, $b'_{Al_2O_3} = 4.76$ Å, and $\alpha'_{Al_2O_3} = 90°$, the calculated in-plane lattice mismatches are 11% and 3% and correspond, respectively, to the following epitaxial relationships: $[010]\text{BZN}\|[1\bar{2}10]Al_2O_3$ and $[001]\text{BZN}\|[10\bar{1}1]Al_2O_3$. Therefore, the lattice mismatch difference depending on the substrate could explain the lower epitaxial quality observed on

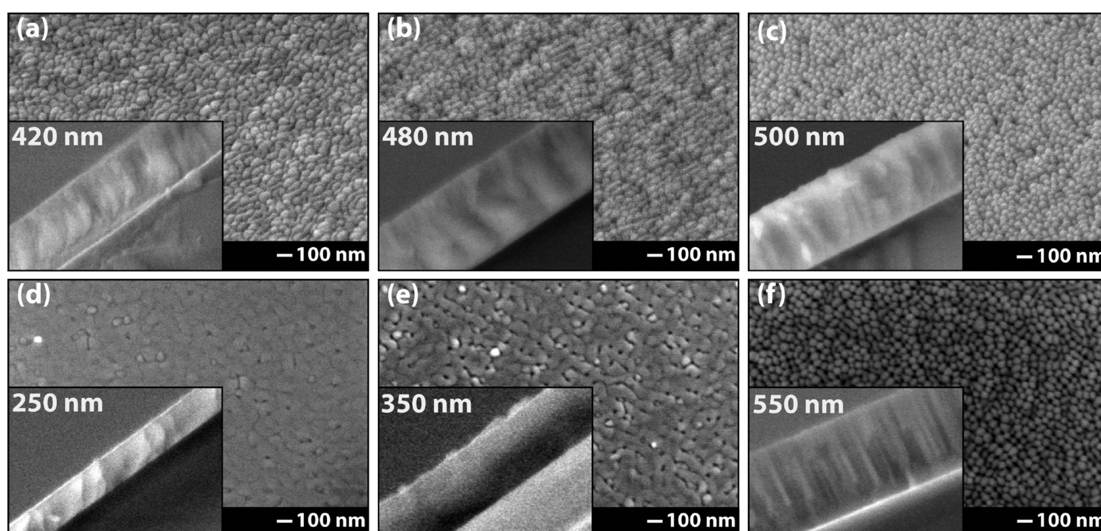

Figure 3. FE-SEM plane views and cross-sectional views of BZN thin films grown on R-plane sapphire (a, b, and c) and on $(100)_{pc}$ LAO (d, e, f) for various deposition pressures: 30 Pa (a, d), 50 Pa (b, e), and 70 Pa (c, f). The film thickness is given in the inset for each micrograph.

the thin film grown on R-plane sapphire. A secondary phase identified as $BiNbO_4$ was detected in a very small amount on LAO at a low deposition pressure but no significant change of the global composition was evidenced by EDS (at an analysis tool accuracy of ≤2%). The deposition temperature was set, for the substrate holder, at the same value for both substrates. Additional punctual pyrometric measurements have evidenced a slightly higher temperature of the LAO substrate than that of the sapphire, at ∼20 °C. The presence of the $BiNbO_4$ secondary phase has already been reported in the literature on thin films deposited by using the PLD process,[12] as well as via the metal−organic decomposition method,[8] where a decomposition of $Bi_{1.5}Zn_{0.5}Nb_{1.5}O_{6.5}$ into $Bi_{1.5}Zn_{0.92}Nb_{1.5}O_{6.92}$ and $BiNbO_4$ has been observed at high temperatures. $BiNbO_4$ has an orthorhombic cell, with a = 4.980 Å, b = 11.700 Å, and c = 5.675 Å (ICDD PDF Card No. 16-0295). In the present study, the secondary phase can be favored by the slightly higher temperature but also by a lower lattice mismatch. $BiNbO_4$ grew with the (010) preferential orientation, which may be induced by the single crystal substrate with calculated in-plane lattice mismatches close to −7% and 6%, respectively, which are defined by:

$$\frac{a_{(BiNbO_4)} - a'_{pc(LAO)}}{a'_{pc(LAO)}} \quad \text{and} \quad \frac{c_{(BiNbO_4)} - a'_{pc(LAO)}}{a'_{pc(LAO)}} \tag{3}$$

In this case, the grains of $BiNbO_4$ could start to crystallize from the surface of the substrate, but there is no evidence that $BiNbO_4$ was present, or not, along the entire film thickness.

Figure 3 shows the plane and cross-section views of the BZN thin films grown on both substrates under the various oxygen pressures. The surface morphology of the layers deposited on R-plane sapphire has the same aspect, regardless of the oxygen pressure, and shows a circular surface plane of the grains. An increase of the average grain size (diameter of cylindrical-like crystallites) from 37 nm (70 Pa) to 77 nm (30 Pa) was observed (see Figure 4). On $(100)_{pc}$ LAO, the same variation of the average grain size was also observed for the thin films grown with an increase from 45 nm (70 Pa) to 80 nm (30 Pa). As opposed to the thin films on sapphire, the surface aspect of the thin films deposited on LAO changes with the decrease of the oxygen pressure in the chamber. Under a pressure of 70 Pa,

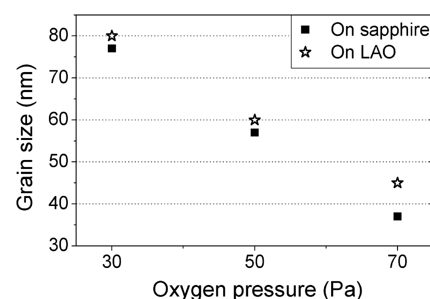

Figure 4. Lateral grain size deduced from the SEM plane view observation of the film deposited (■) on sapphire and (☆) on LAO under different oxygen pressures: 30, 50, and 70 Pa.

the film was comprised of small grains (45 nm) that appeared to be disconnected. When the deposition pressure decreased to 50 Pa, the morphology changed suddenly and the films appeared more continuous, dense, and smooth and were comprised of grains with an average diameter of 60 nm. Then, the decrease of the oxygen pressure to 30 Pa increased the grain size to 80 nm.

The evolution of the microstructure versus the oxygen pressure was reported in many cases (for example, on $Bi_{1.5}Zn_{1.0}Nb_{1.5}O_7$[15] and on graded $(Ba_{1-x}Sr_x)TiO_3$).[22] This evolution could be explained by the Thornton Structure Zone Model.[23] The change of microstructure is ascribed to the properties of the species appearing on the surface substrate. It is known that the ablated species, which are ejected from the target, lose kinetic energy. This is essentially due to scattering by the oxygen molecules. When the oxygen pressure increases, the species reach the substrate with a lower kinetic energy; therefore, their surface mobility decreases, which involves a smaller grain size.[24]

Moreover, the thickness of the films deposited on the two substrates decreases with the oxygen pressure, especially on LAO (see Figure 3). In the case of the highest pressure, the film is clearly comprised of columnar grains (diameter ⌀ × length l ≈ 45 nm × 550 nm), which grow from the film/substrate interface to the surface and show homogeneous nanoporosity. This porosity decreases as the pressure decreases (see Figures 3d, 3e, 3f). The difference in thickness, relative to the

deposition pressure, could be explained by two phenomena, which are directly linked to the effect of the oxygen pressure on the plasma and on the particle kinetic energy. As explained previously, at a low oxygen pressure, species reach the substrate with a higher kinetic energy, which promotes densification. In addition, the increase of the deposition pressure induces some changes on the spatial extent of the plasma, which favors plasma confinement. Therefore, an equivalent amount of matter from the target impinges the substrate over a smaller area, which contributes to an increase in the growth rate.[24−26]

In this study, the oxygen pressure clearly affects the grain size of the BZN thin films grown on both substrates and also the growth mechanisms, which induce various morphologies.

Optical and Dielectric Properties. Figure 5 represents the optical refractive indexes (n) and the microwave dielectric constant (ε_r) measured on BZN films grown on R-plane sapphire. The variation of n near the film/substrate interface (n_{bottom}) and near the surface (n_{top}) is displayed in Figure 5a as a function of the wavelength. A graded layer model was used to fit the spectroscopic ellipsometry data. A variation of the refractive index was observed along the thickness of the layer. The indicated values are in the same range as those reported in the literature.[13,26,27] Figure 5b shows the variations of n (n_{top} and n_{bottom}) at 630 nm, and ε_r at 10 GHz, of the BZN thin films versus the grain size and the oxygen deposition pressure.

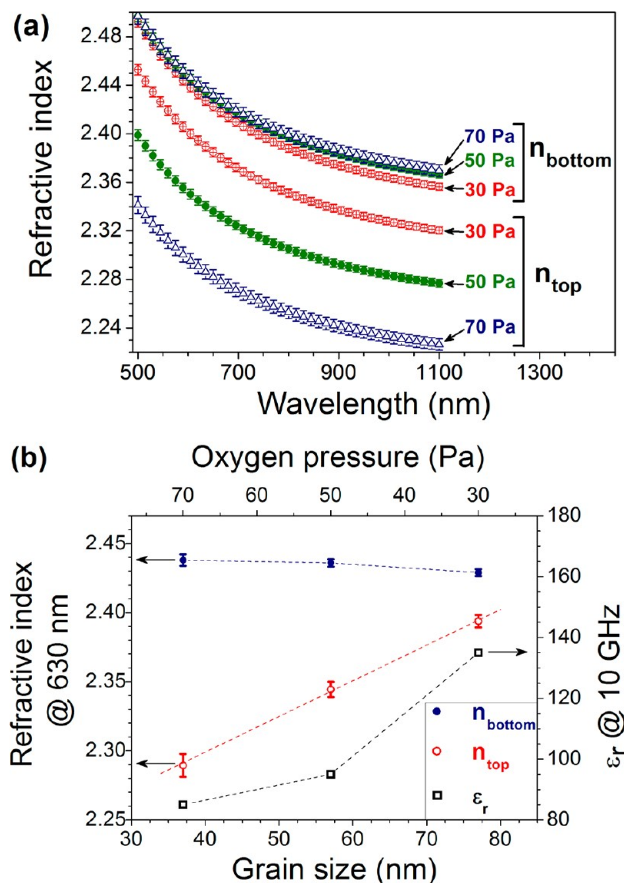

Figure 5. Optical and dielectric properties of the BZN/R-plane sapphire thin films: (a) n_{bottom} (interface between the thin film and substrate) and n_{top} (surface) refractive indexes of the BZN films grown under various oxygen deposition pressures (70, 50 and 30 Pa); (b) refractive index (@ 630 nm) and dielectric constant (@ 10 GHz) of the BZN films versus grain size.

Regarding the refractive index at the film/substrate interface (n_{bottom}), the three pressures of oxygen led to an equivalent value of ~2.435 (at 630 nm), which was close to the value of the bulk material ($n \approx 2.4$).[13] It seems that the film/substrate interface layer is quasi-independent of the oxygen deposition pressure. The n_{top} refractive indexes (surface of the thin film) are lower than the n_{bottom} refractive indexes and undergo a linear-like variation, as a function of the pressure and grain size, observed with refractive indexes of 2.39, 2.34, and 2.29 for the thin films grown under 30, 50, and 70 Pa, respectively, which also correspond to average grain sizes of 77, 57, and 37 nm, respectively. There is no significant variation of the bottom refractive index while a linear-like relationship between the top refractive index and the average grain size is evidenced.

The BZN thin films show a dielectric permittivity ranging between 85 and 135. The effective loss tangent ($\tan \delta_{eff} = \varepsilon''_{eff}/\varepsilon'_{eff}$) was similar to that measured on bare sapphire substrates. Therefore, BZN thin films should show a very low dielectric loss, not far from that of the sapphire substrate (~10^{-4} at 10 GHz). This explains why it was not possible to determine the intrinsic BZN loss from the scattering parameters. For comparison, a dielectric constant (ε_r) of 200 has been reported in other studies for randomly oriented BZN thin films deposited on Pt-coated Si measured at lower frequencies (10 kHz and 100 kHz).[4,16] A dielectric permittivity of 150 at 10 GHz was reported by Booth et al.[28] for polycrystalline $Bi_{1.5}Zn_1Nb_{1.5}O_7$ thin films grown on a *c*-plane sapphire substrate by RF sputtering. The difference in dielectric permittivity is explained by the different given frequency, and by the structural properties of the measured BZN thin films. Furthermore, it has been shown that a decrease of Bi^{3+} in site A leads to a decrease of the dielectric permittivity,[29] whereas a decrease of the Zn^{2+} content involves a higher permittivity.[8] In the present work, the variation of the permittivity with the oxygen deposition pressure could not be explained by a difference in the cation composition, because the films have the same composition, such as revealed by EDS. An increase of the lateral grain size, correlated with a decrease of the oxygen pressure, involves an increase of the dielectric constant from 85 to 135. Similarly, an increase of the dielectric permittivity from 120 to 180 at 10 kHz when the oxygen deposition pressure decreases from 50 Pa to 10 Pa has been observed on $Bi_{1.5}Zn_1Nb_{1.5}O_7$ thin films grown on Pt-coated Si.[15] The authors attributed this variation to the variation of stress, (111) preferential orientation, and microstructure (shape of grains, grain size, and thickness) (which demonstrated a strong dependency on the oxygen pressure). Other examples were reported such as a study on $SrTiO_3$ thin films, which has evidenced an increase of the dielectric constant with the increase of the grain size.[30]

In order to provide a qualitative explanation for the dependence of both the refractive index in the visible range and the dielectric permittivity in the microwave range on the grain size, the Bruggeman effective medium approximation[31,32] can be used:

$$f_b\left(\frac{\varepsilon_b - \varepsilon_m}{\varepsilon_b + 2\varepsilon_m}\right) + (1 - f_b)\left(\frac{\varepsilon_g - \varepsilon_m}{\varepsilon_g + 2\varepsilon_m}\right) = 0 \tag{4}$$

where ε_m, ε_g, and ε_b are the medium effective dielectric function, the dielectric function of the grains, and the counterpart of the grain boundaries, respectively. f_b is the "volume" fill fraction of the grain boundaries. It is well-known

that spectroscopic ellipsometry is a powerful characterization technique. With a good understanding, correct modeling and also the use of complementary techniques, even the grain size can be correlated with the dielectric function.[33−37] Usually, the dielectric function (the squared refractive index) of a grain is larger than that of the grain boundary, since the dielectric function is proportional to the atomic density[38,39] and the local or extended defects identify the grain boundaries.[40] Therefore, the smaller the grain size, the higher the density of the grain boundaries (higher f_b), and the smaller the corresponding refractive index. In order to also try to explain why, at the thin film/substrate interface, there is an optically denser material, we have taken into account the growth consideration. According to the columnar shape of the grains which grow perpendicular to the substrate surface, it can be assumed that the growth process is a three-dimensional process (Volmer−Weber model). At the interface, because of the lateral compressive stress undergone by the BZN cells, as well as the stress between two adjacent growing islands, it can be envisaged that the forming layer will have a higher atom concentration, i.e., a higher density, than the relaxed top layer. Moreover, because of the same lateral compressive stress, the atom density along the grain boundaries in the nucleation layer might be higher than the atom density inside the grains.

In this study, the thin films grown on R-plane sapphire show a roughly similar density whatever the pressure (see Figure 3). Consequently, the behavior of the optical and dielectric properties could be explained by the variation of the microstructure along the film thickness and between samples, in which the grain size changes under the oxygen deposition pressure (grain size and density of grain boundaries).

Figure 6a represents the dispersion of the refractive index of the BZN films grown on LAO at various oxygen deposition pressures as a function of the wavelength, whereas Figure 6b shows the refractive indexes at 630 nm versus the grain size and the oxygen pressure. In contrast to the results obtained on R-plane sapphire, no variation of the refractive index along the film thickness is observed. This result shows the homogeneous growth of the films. BZN films have a similar refractive index dispersion with absolute values, which are slightly higher than the bottom refractive indexes of the BZN films grown on R-plane sapphire. These differences might be attributed to the specific growth characteristics induced by each substrate, which lead to different microstructures, and/or to the presence of the $BiNbO_4$ secondary phase (a higher index material with a value close to 2.5).[41] As observed on sapphire, the refractive index of BZN thin films grown on LAO increases from 2.47 (70 Pa) to 2.5 (30 Pa) when the average grain size increases from 45 nm to 70 nm (see Figure 6b). Although the refractive index—each atom's volume density—grain size recurrence seems to govern the characteristics of the thin films described, we cannot exclude contributions from possible slight stoichiometry differences between samples as well as stoichiometry in-depth profiles, which usually occur when a single source (target) is used.[42,43] Also, the presence of $BiNbO_4$ at the lowest deposition pressures can contribute to increasing the refractive index.

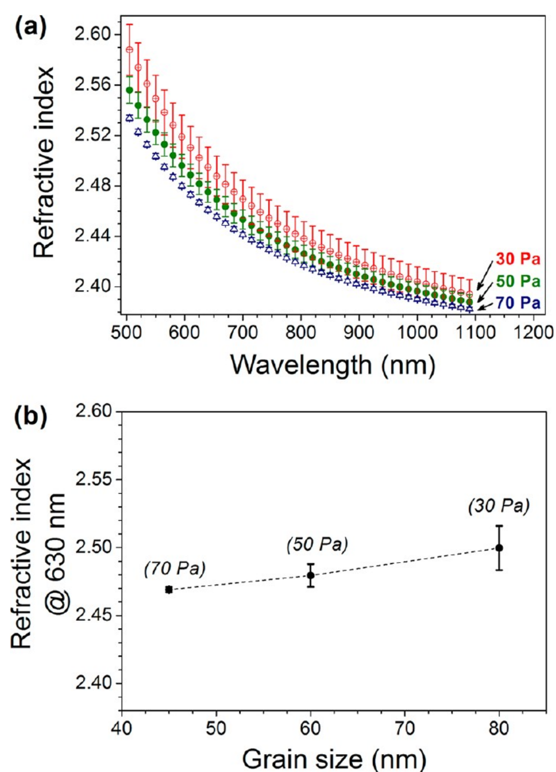

Figure 6. Optical properties of the BZN/$(100)_{pc}$ LAO thin films: (a) refractive index of the BZN films grown under various oxygen deposition pressures (70, 50, 30 Pa); (b) refractive index of the BZN films versus grain size.

■ CONCLUSION

(100) epitaxial-like grown BZN cubic pyrochlore thin films have been deposited on R-plane sapphire and $(100)_{pc}$ $LaAlO_3$ substrates. The microstructure of the thin films is sensitive to the substrate and to the oxygen deposition pressure. When the pressure decreases from 70 Pa to 30 Pa, the lateral grain size increases from 37 nm to 77 nm and from 45 nm to 80 nm on sapphire and $LaAlO_3$, respectively. The influence of the microstructure on optical and dielectric properties was emphasized. Optical studies have shown that, in contrast with $LaAlO_3$, the films deposited on sapphire display a graded refractive index from the film/substrate interface to the surface. The refractive index shows a quasi-linear dependence on grain size (from 2.29 to 2.39 on sapphire). Moreover, a strong correlation between the characteristics measured by spectroscopic ellipsometry on bare thin films (n in the optical range) and on coplanar devices in the microwave range (ε_r at 10 GHz) was evidenced. Although the dependence of the refractive index on grain size cannot be generalized to other thin films and/or other deposition processes, the unexpected optical properties−grain-size relationship might be understandable, according to the present work.

■ AUTHOR INFORMATION

Corresponding Author

*E-mail addresses: stephanie.deputier@univ-rennes1.fr (S.D.), ac_galca@infim.ro (A.C.G.).

Notes

The authors declare no competing financial interest.

■ ACKNOWLEDGMENTS

The authors acknowledge the Region of Bretagne (PRIR Discotec) and the Romanian Ministry of Education, Research, Youth and Sport-National Authority for Scientific Research (PN-II-RU-TE-2011-3-0016 Project) for their financial support, I. Peron and F. Gouttefangeas for the EDS analyses, and J. Le

Lannic for the FE-SEM images at CMEBA of the University of Rennes 1.

■ REFERENCES

(1) Gevorgian, S. *Ferroelectrics in Microwave Devices, Circuits and Systems*; Springer: London, 2009.
(2) Kim, H.-S.; Kim, H.-G.; Kim, I.-D.; Kim, K.-B.; Lee, J.-C. *Appl. Phys. Lett.* **2005**, *87*, 212903.
(3) Simon, Q.; Corredores, Y.; Castel, X.; Benzerga, R.; Sauleau, R.; Mahdjoubi, K.; Le Febvrier, A.; Députier, S.; Guilloux-Viry, M.; Zhang, L.; Laurent, P.; Tanné, G. *Appl. Phys. Lett.* **2011**, *99*, 092904.
(4) Ren, W.; Trolier-McKinstry, S.; Randall, C. A.; Shrout, T. R. *J. Appl. Phys.* **2001**, *89*, 767−774.
(5) Lu, J.; Stemmer, S. *Appl. Phys. Lett.* **2003**, *83*, 2411−2413.
(6) Sudheendran, K.; Raju, K. C. J. *Ceram. Int.* **2008**, *34*, 897−900.
(7) Nino, J. C.; Lanagan, M. T.; Randall, C. A. *J. Appl. Phys.* **2001**, *89*, 4512−4516.
(8) Thayer, R. L.; Randall, C. A.; Trolier-McKinstry, S. *J. Appl. Phys.* **2003**, *94*, 1941−1947.
(9) Hong, Y. P.; Ha, S.; Lee, H. Y.; Lee, Y. C.; Ko, K. H.; Kim, D.-W.; Hong, H. B.; Hong, K. S. *Thin Solid Films* **2002**, *419*, 183−188.
(10) Lee, Y. C.; Hong, Y. P.; Kim, D. M.; Ko, K. H. *Electron. Lett.* **2006**, *42*, 851−853.
(11) Cao, L. Z.; Fu, W. Y.; Wang, S. F.; Wang, Q.; Sun, Z. H.; Yang, H.; Cheng, B. L.; Wang, H.; Zhou, Y. L. *J. Phys. D: Appl. Phys.* **2007**, 2906.
(12) Zhang, X.; Ren, W.; Shi, P.; Tian, A.; Xin, H.; Chen, X.; Wu, X.; Yao, X. *Appl. Surf. Sci.* **2010**, *256*, 6607−6611.
(13) Cheng, J.-G.; Wang, J.; Dechakupt, T.; Trolier-McKinstry, S. *Appl. Phys. Lett.* **2005**, *87*, 232905.
(14) Sudheendran, K.; Singh, M. K.; Raju, K. C. J.; Katiyar, R. S. *Solid State Commun.* **2010**, *150*, 1928−1931.
(15) Zhang, X.; Ren, W.; Shi, P.; Chen, X.; Wu, X. *Appl. Surf. Sci.* **2010**, *256*, 1861−1866.
(16) Le Febvrier, A.; Députier, S.; Bouquet, V.; Demange, V.; Ollivier, S.; Galca, A. C.; Dragoi, C.; Radu, R.; Pintilie, L.; Guilloux-Viry, M. *Thin Solid Films* **2012**, *520*, 4564−4567.
(17) Valant, M.; Davies, P. K. *J. Am. Ceram. Soc.* **2000**, *83*, 147−153.
(18) Cauchy, A. L. *Bull. Sci. Math.* **1830**, *14*, 6−10.
(19) Zhang, J.; Hsiang, T. Y. *PIERS Online* **2007**, *3*, 1102−1106.
(20) Carlsson, E.; Gevorgian, S. *IEEE Trans. Microwave Theory Technol.* **1999**, *47*, 1544−1552.
(21) Wang, X.; Wang, H.; Yao, X. *J. Am. Ceram. Soc.* **1997**, *80*, 2745−2748.
(22) Zhu, X. H.; Chan, H. L. W.; Choy, C. L.; Wong, K. H. *Appl. Phys. A: Mater. Sci. Process.* **2005**, *80*, 591−595.
(23) Thornton, J. A. *J. Vac. Sci. Technol.* **1974**, *11*, 666−670.
(24) Bäuerle, D. *Laser Processing and Chemistry*; Springer: Heidleberg, Germany, 2011.
(25) Gonzalo, J.; Gómez San Román, R.; Perrière, J.; Afonso, C. N.; Pérez Casero, R. *Appl. Phys. A: Mater. Sci. Process.* **1998**, *66*, 487−491.
(26) Biegalski, M.; Thayer, R.; Nino, J.; Trolier-McKinstry, S. Dielectric properties of capacitor materials in the optical frequency range. In *Proceedings of the 13th IEEE International Symposium on Applications of Ferroelectrics, ISAF 2002*, Nara, Japan, May 28−June 1, 2002; pp 7−10.
(27) Sudheendran, K.; Ghanashyam Krishna, M.; Raju, K. *Appl. Phys. A: Mater. Sci. Process.* **2009**, *95*, 485−492.
(28) Booth, J. C.; Orloff, N. D.; Cagnon, J.; Lu, J.; Stemmer, S. *Appl. Phys. Lett.* **2010**, *97*, 022902.
(29) Wang, Q.; Wang, H.; Yao, X. *Ceram. Int.* **2009**, *35*, 143−146.
(30) He, S.; Li, Y.; Liu, X.; Tao, B.; Li, D.; Lu, Q. *Thin Solid Films* **2005**, *478*, 261−264.
(31) Kooij, E. S.; Wormeester, H.; Galca, A. C.; Poelsema, B. *Electrochem. Solid-State Lett.* **2003**, *6*, B52−B54.
(32) Curecheriu, L.; Buscaglia, M. T.; Buscaglia, V.; Zhao, Z.; Mitoseriu, L. *Appl. Phys. Lett.* **2010**, *97*, 242909−3.
(33) Feng, G. F.; Zallen, R. *Phys. Rev. B* **1989**, *40*, 1064−1073.
(34) Boultadakis, S.; Logothetidis, S.; Ves, S. *J. Appl. Phys.* **1992**, *72*, 3648−3658.
(35) Boultadakis, S.; Logothetidis, S.; Ves, S.; Kircher, J. *J. Appl. Phys.* **1993**, *73*, 914−925.
(36) Nguyen, H. V.; Collins, R. W. *Phys. Rev. B* **1993**, *47*, 1911−1917.
(37) Suzuki, T.; Adachi, S. *Jpn. J. Appl. Phys.* **1993**, *32*, 4900−4906.
(38) Kintaka, Y.; Kuretake, S.; Hayashi, T.; Tanaka, N.; Ando, A.; Takagi, H. *J. Am. Ceram. Soc.* **2011**, *94*, 1551−2916.
(39) Polosan, S.; Galca, A. C.; Secu, M. *Solid State Sci.* **2011**, *13*, 49−53.
(40) Ong, H. C.; Dai, J. Y.; Hung, K. C.; Chan, Y. C.; Chang, R. P. H.; Ho, S. T. *Appl. Phys. Lett.* **2000**, *77*, 1484−1486.
(41) Popolitov, V. I.; Lobachev, A. N.; Peskin, V. F. *Ferroelectrics* **1982**, *40*, 9−16.
(42) Galca, A. C.; Stancu, V.; Husanu, M. A.; Dragoi, C.; Gheorghe, N. G.; Trupina, L.; Enculescu, M.; Vasile, E. *Appl. Surf. Sci.* **2011**, *257*, 5938−5943.
(43) Cernea, M.; Trupina, L.; Dragoi, C.; Galca, A.-C.; Trinca, L. *J. Mater. Sci.* **2012**, *47*, 6966−6971.